The spatial distribution of the paramagnetically aligned moments in the high-temperature insulating phase of V_2O_3

2001 J. Phys.: Condens. Matter 13 10261

(http://iopscience.iop.org/0953-8984/13/45/312)

INSTITUTE OF PHYSICS PUBLISHING JOURNAL OF PHYSICS: CONDENSED MATTER

J. Phys.: Condens. Matter **13** (2001) 10261–10268 PII: S0953-8984(01)27943-0

The spatial distribution of the paramagnetically aligned moments in the high-temperature insulating phase of V_2O_3

P J Brown[1,2], **M M R Costa**[3] **and K R A Ziebeck**[2]

[1] Institut Laue–Langevin, BP156 38042 Grenoble, France
[2] Department of Physics, Loughborough University, Leicestershire LE11 3TU, UK
[3] Departamento de Fizica, Universidade de Coimbra, 3000 Coimbra, Portugal

Received 16 August 2001, in final form 3 October 2001
Published 26 October 2001
Online at stacks.iop.org/JPhysCM/13/10261

Abstract

The spatial distribution of the magnetization induced in V_2O_3 at 600 K by a field of 9 T has been determined using polarized neutron diffraction. At this temperature V_2O_3 has the rhombohedral corundum structure and behaves as an insulator, whereas at lower temperature the same structure exhibits metallic conduction. The susceptibilities of the conducting and insulating states are similar, $\simeq 10^{-5}$ emu g^{-1}, and the moment aligned by 9 T at 600 K is 0.014 μ_B/V. The magnetic structure factors were determined from the polarization dependence of the intensities of the Bragg reflections. The results show that there is a significant change in the paramagnetic moment distribution between 180 K and 600 K. At the higher temperature the moment distribution around the V atoms has nearly cylindrical symmetry about the triad axis. The negative moment associated with the oxygen sites which was induced at 180 K was also found at 600 K where it amounts to some 5% of the total moment.

1. Introduction

The Magneli series V_nO_{2n-1} is a group of mixed-valence compounds which can be described as having $n - 2$ V^{4+} ions and two V^{3+} ions per formula unit. The two end-members of the series V_2O_3 ($n = 2$) and VO_2 ($n \to \infty$) both undergo metal–insulator transitions on cooling. In both cases the transition is accompanied by lattice distortions and changes in magnetic susceptibility. In V_2O_3 the metal-to-insulator transition at low temperature is associated with a structural phase transition and the onset of antiferromagnetism. It has been shown [1] that this transition is accompanied by orbital ordering. Inelastic neutron scattering measurements have shown that dynamic short-range magnetic order persists in the metallic phase of V_2O_3 [2]. A recent polarized neutron diffraction study [3] has shown that in the metallic phase, just above T_N the moment which can be induced on the V atoms by an applied field is almost entirely due to electrons in the doubly degenerate orbitals which are thought to give rise to orbital

ordering. At higher temperatures, around 550 K, V_2O_3 undergoes a gradual transition back to an insulating state. This second transition can be changed to an abrupt one between two corundum structures with different lattice parameters, by doping with chromium [4, 5]. It has all the characteristics of a Mott transition. It is argued that the gradual transition in pure V_2O_3 is due to supercritical behaviour associated with the critical point for the Mott transition in the P–T phase diagram. The high-temperature insulating phase of V_2O_3 differs fundamentally from the low-temperature one in that it is neither antiferromagnetic nor distorted. It is thought that its low conductivity is due to greater localization of the d electrons associated with the increasing V–V distance.

The magnetic susceptibility of V_2O_3 increases sharply by a factor of about two at the low-temperature insulator-to-metal transition [6]. Between 165 and 400 K the susceptibility decreases slowly to about 75% of its maximum value. It then remains nearly constant from 400 to 600 K, a temperature range in which the resistivity increases by about a factor of ten. The molar susceptibility of V_2O_3 at 600 K is 1.7×10^{-3} emu mol^{-1}, only some 20% less than its value at 180 K. It is therefore quite feasible to use polarized neutrons to determine the distribution of magnetization induced by an applied field at 600 K with as good precision as was obtained in the previous experiment at 180 K [3]. A comparison between the two distributions should help in understanding the evolution with temperature of the electronic structure of this well studied but poorly understood compound.

2. Experimental procedure

The experiments were carried out using the same two crystals as in our previous study [3]. They had dimensions $\simeq 4 \times 3 \times 3$ mm and were mounted one with a $\langle 10\,.\,0 \rangle$ and the other with a $\langle 1\bar{1}\,.\,0 \rangle$ axis vertical.

2.1. Unpolarized neutron diffraction

The evolution with temperature of the structural parameters of V_2O_3 has already been studied [7]. However, since the values of the nuclear structure factors are essential for the interpretation of the polarized neutron measurements, it was decided to confirm these for our particular crystals by making integrated intensity measurements at 300 and at 600 K. The extinction parameters for these crystals had already been determined in the previous experiment so the intensities were only measured at a single wavelength (0.84 Å). The $\langle 10\,.\,0 \rangle$-axis crystal (A) was fixed inside a resistive wire furnace which was mounted on the χ-circle of the four-circle diffractometer D9 at ILL. The integrated intensities of some 900 reflections with $(\sin\theta)/\lambda < 0.90$ Å^{-1} were measured at 600 K and at 300 K. Averaging over symmetrical equivalents yielded 273 independent reflections which were used in least-squares refinements to determine the positional and temperature parameters given in table 1. The results of structure refinements based on x-ray data [7] are also shown in table 1. The positional parameters agree within their standard deviations at 600 K, although on lowering the temperature the neutron data appear to show larger changes than do the x-ray results. As expected, the accuracy of determination of the positional parameter of V, which has a very small neutron scattering length, is better from the x-ray data; whereas the neutron data determine the oxygen position with better precision. In the subsequent analysis the V z-coordinate at 600 K is taken as 0.388 18 (the x-ray value) and the O x-coordinate as 0.308 97 (the neutron value).

Table 1. Crystallographic data and temperature dependence of the structural parameters of V_2O_3.

Space group:	$R\bar{3}c$	
Hexagonal unit cell	$a = 4.952$ Å	$c = 14.002$ Å
Atomic positions:	12 V at 12(c), $00z$	18 O at 18(e), $x0\frac{1}{4}$

	V			O		
T (K)	z[a]	z	B (Å^{-2})	x[a]	x	B (Å^{-2})
600	0.34818(4)	0.3480(6)	0.49(8)	0.3087(4)	0.30897(14)	0.723(13)
300	0.34782(5)	0.3464(5)	0.21(5)	0.3095(5)	0.31193(10)	0.443(9)
180	0.34733(4)	0.3455(3)		0.3103(5)	0.31255(5)	0.413(7)

[a] Values from [7] for 212, 300, and 600 K.

2.2. Polarized neutron measurements

Polarized neutron flipping ratios were measured on the D3 polarized neutron diffractometer at ILL. The two crystals were mounted in turn in a special high-temperature insert, containing a heating coil, for the 10 T split-pair superconducting magnet. With this insert, and by maintaining a vacuum of $\simeq 10^{-4}$ mb in the sample chamber, it was possible to reach a sample temperature of 600 K without endangering the cryomagnet's indium seals. The measurements were made in a field of 9 T, for the same reflections from both crystals as had proved to be measurable with reasonable precision at 180 K. The higher field available, 9 T compared to 4.6 T, more than compensated for the decrease in the susceptibility, and it was possible to determine the magnetic structure factors of most reflections with a statistical precision better than 5×10^{-3} μ_B/hexagonal cell in the ten-day experiment.

The magnetic structure factors were calculated from the measured flipping ratios using the structure parameters deduced from the structure refinements. The procedure used takes into account incomplete polarization of the incident beam, the inclination of the scattering vector to the magnetic field direction, and extinction. Each magnetic structure factor was obtained from the average of at least two equivalent reflections. A small correction for diamagnetic scattering, which was in almost all cases less than the standard deviation, was applied. The final list of observed structure factors is given in table 2 in which the data from the two crystals have been merged. The observed structure factors of reflections which were measured for the two crystals were found to be in good agreement.

3. Analysis of the results

In order to judge whether the measurements can distinguish any significant change in the shape of the magnetization distribution between 180 and 600 K, the hypothesis that a single scale factor related the two sets was tested. The mean scale factor between the 22 reflections for which measurements at both temperatures were available was 1.60. A χ^2-test on the differences between the observations, once scaled together, indicated that the probability of the two magnetization distributions being the same was less than 0.1%. Further analysis of the high-temperature data was therefore pursued, using the same techniques as were used for the 180 K data [3]. The best fit between the observed magnetic structure factors and the scattering due to the sum of spherically symmetric V^{3+} ions at the V sites was obtained with a V moment of 0.014 μ_B.

Table 2. Observed and calculated magnetic structure factors for V_2O_3.

				Observed[a]		Calculated[a]		
h	k	l	$(\sin\theta)/\lambda$	180 K[b]	600 K	Spherical	Unrestricted	Quadrupole
1	0	2	0.1367	−42(2)	−43.8(1.3)	−45.1	−41.7	−42.9
1	0	$\bar{4}$	0.1844	−72(2)	−85.4(1.5)	−87.7	−89.4	−91.1
1	1	0	0.2019	96(9)	99(2)	105.9	99.9	100.3
0	0	6	0.2143	111(7)	104.7(1.5)	82.4	101.1	100.5
1	1	3	0.2286	−2(3)	−2(2)	0.0	−5.8	−5.5
2	0	$\bar{2}$	0.2439	−28(3)	−30(4)	−28.6	−26.8	−26.6
2	0	4	0.2734	−42(5)	−53(3)	−56.4	−55.0	−53.2
1	1	6	0.2944	57(9)	56(2)	53.5	55.9	54.9
1	0	8	0.3085	2(8)	5(3)	12.0	16.4	15.3
2	1	$\bar{1}$	0.3105	−10(5)	−1(2)	0.0	−1.1	−0.9
2	1	2	0.3166	−14(7)	−16(2)	−18.8	−17.1	−15.6
2	1	$\bar{4}$	0.3399	−11(10)	−11(16)	−37.3	−33.8	−32.4
3	0	0	0.3498	29(8)	42(4)	45.4	37.4	31.1
2	1	5	0.3564	−2(13)	6(4)	0.0	0.7	0.7
2	0	$\bar{8}$	0.3688	12(12)	−7(9)	8.0	10.4	10.3
1	1	9	0.3796	−7(4)	−4(3)	0.0	1.2	1.9
2	1	$\bar{7}$	0.3970	−6(9)	13(12)	0.0	−1.4	0.5
2	2	0	0.4039	27(5)	31(4)	30.6	27.5	20.4
3	0	6	0.4102	24(8)	29(3)	24.0	27.1	23.2
3	0	$\bar{6}$	0.4102	31(6)	36(8)	24.0	22.4	23.2
2	2	3	0.4178	−11(4)	−2(2)	0.0	−0.7	1.3
3	1	1	0.4219	−8(8)	−1(7)	0.0	0.0	−0.3
2	0	10	0.4265	−31(8)	−37(5)	−23.2	−38.1	−33.4
0	0	12	0.4285	22(3)	13(4)	9.9	21.8	16.3
3	1	4	0.4440	−20(6)	−17(5)	−16.9	−16.8	−11.6
2	2	6	0.4572	20(5)	13(3)	16.2	14.5	12.4
2	1	$\bar{10}$	0.4719	9(4)	−22(17)	−15.7	−21.8	−21.6
1	1	12	0.4737	9(4)	9(4)	6.7	15.1	12.4

[a] The structure factors are in units of 10^{-3} μ_B/hexagonal unit cell.
[b] Values from [3] scaled by 1.6.

3.1. Maximum-entropy reconstruction

In order to obtain some idea of the distribution of induced magnetization in real space the maximum-entropy (ME) algorithm [8] was used to reconstruct a difference density in the same way as in our previous paper [3]. The calculated density displays the differences between the observed magnetic structure factors and those calculated for V^{3+} spherical 3d moments of 0.014 μ_B centred at each V site. The section of this reconstruction parallel to (01 . 0) passing through the origin is shown in figure 1.

The most significant feature in the ME map is a negative density centred on the triad axis about 0.7 Å from the V^{3+} ion. It is on the side remote from the near V^{3+} neighbour on the same triad axis and is extended in the (00 . 1) plane. There is no corresponding feature on the other side of the V^{3+} ion. The ME reconstruction has other weaker features, both positive and negative, including a diffuse negative region near to the O^{2-} ion.

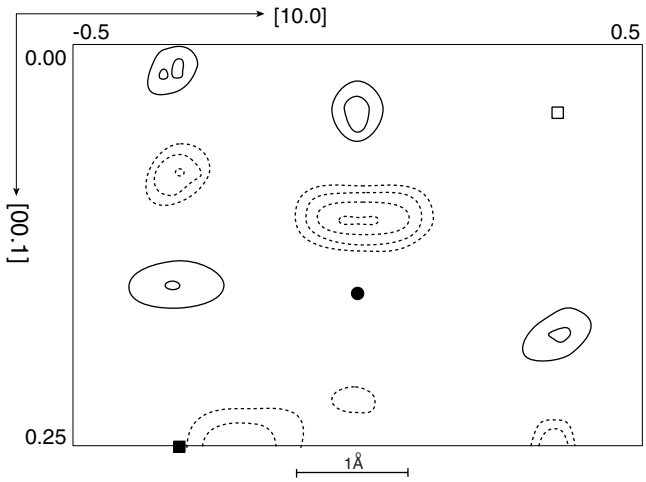

Figure 1. The section, parallel to (01 . 0) passing through the origin, of the maximum-entropy reconstruction of the difference between the observed magnetization distribution and that due to the spherically symmetric V^{3+} spin. ● marks the position of the V^{3+} ion, ■ that of the O^{2-} ion in the plane of the section and □ that of the O^{2-} ion which is 0.1 Å below it. The contours are logarithmically spaced with a factor of two between successive levels. The highest contour is at 0.4×10^{-3} μ_B Å^{-3}.

3.2. Multipole fits to the density

A more quantitative analysis of the data can be made by modelling the density by the sum of multipole functions, having appropriate radial densities, centred on the atomic sites. The real combinations of even multipole functions permitted by the trigonal symmetry of the V site in V_2O_3 up to order 4 are:

$$\begin{aligned} &Y(00) = Y_0^0 \qquad Y(20) = Y_2^0 \qquad Y(40) = Y_4^0 \\ &Y(43+) = (Y_4^3 + Y_4^{3*})/\sqrt{2} \qquad Y(43-) = \mathrm{i}(Y_4^3 - Y_4^{3*})/\sqrt{2}. \end{aligned} \tag{1}$$

The amplitudes of these functions, together with that of a $Y(00)$ 2p function, centred on the O sites, were allowed to vary in a multipole refinement using the observed magnetic structure factors as data. Some flexibility was allowed in the radial density around V by modelling the form factor for the spherically symmetric density as

$$f_{sph}(k) = \langle j_0(k) \rangle + a_{orb} \langle j_2(k) \rangle. \tag{2}$$

This is the dipole approximation to the form factor [9] for an ion with g-factor $2/(1 - a_{orb})$, but the parameter a_{orb} may also model small expansions (negative a_{orb}) or contractions (positive a_{orb}) of the radial distribution which are not necessarily the consequence of orbital magnetization.

The results of refinements carried out with a series of different constraints on the allowed parameters are shown in table 3. In all cases a significant improvement in the goodness of fit was obtained by allowing a moment on the O^{2-} ion, but that obtained by introducing the orbital parameter a_{orb} was only marginal. For the multipoles the only really significant amplitude is that of $Y(20)$. The data are not sensitive to the values of the hexapoles. The coefficients of $Y(43-)$ and $Y(43+)$ are about equal and of opposite sign. A multipole fit using only monopoles and quadrupoles gives a fit which is almost as good as that in which the hexapoles are included indicating that the V density is nearly cylindrically symmetrical about the c-axis. The structure

Table 3. Parameters obtained in least-squares fits to the magnetic structure factors induced by 9 T at 600 K in V_2O_3.

Parameter:	Spherical			Unrestricted			Quadrupoles only	
V μ	14.8(4)	14.2(4)	13.2(6)	14.2(3)	14.0(3)	13.3(5)	14.2(3)	13.9(2)
V orbital			4(2)			3(2)		
O 2p μ		−1.0(3)	−1.0(3)		−0.6(2)	−0.6(2)		−0.7(2)
V $Y(20)$				−4.1(8)	−3.6(7)	−3.6(7)	−4.2(8)	−3.6(7)
V $Y(40)$				6(3)	3(3)	3(3)		
V $Y(43+)$				3(3)	2(3)	2(3)		
V $Y(43-)$				−5(4)	−4(4)	−2(4)		
χ^{2} [b]	9.51	6.03	6.12	3.81	3.16	2.91	4.13	3.06

[a] The parameters are given in units of 10^{-3} μ_B/atom.
[b] $\chi^2 = \left[\sum_{\text{observations}}(F_{obs} - F_{calc})^2/(\Delta F_{obs})^2\right]/(n_{\text{observations}} - n_{\text{parameters}})$.

factors calculated using the parameters given in columns 2, 5, and 7 of table 3 are listed in table 2 where they may be compared with the observed values.

4. Discussion

The results of the multipole refinements given in table 3 show that the radial distribution of magnetization around the V^{3+} ions is close to that of the V^{3+} free ion, and that any orbital contribution to the magnetization is small. On the other hand the models in which magnetization is permitted to reside on the O^{2-} ions always give a significantly better fit than those in which it is not; leading to the conclusion that there is a negative magnetization around the O^{2-} ions amounting to some 5% of the total moment. The presence of such a reverse-polarized magnetization implies some degree of exchange coupling between states which are paramagnetically active at the Fermi surface.

The multipole analysis shows that none of the hexapoles is really significant. This is partly because the contribution to the scattering of the hexapoles depends on the form factor $\langle j_4 \rangle$ which has a maximum value of only 0.096 and is less than this for all reflections measured. It may however be noteworthy that the coefficients of $Y(43+)$ and $Y(43-)$ are always of opposite sign. The combination of multipoles derived does not seem to be compatible with a simple combination of functions into which the cubic e_g and t_{2g} states are split by a trigonal field [3] since for those particular linear combinations of d functions a negative coefficient for $Y(20)$ implies a positive one for $Y(43-)$. More generally, the combinations of d functions with trigonal symmetry may be written as

$$\begin{aligned} &a_1: && Y_2^0 \\ &e_1(1): && aY_2^2 + bY_2^{-1} \\ &e_1(2): && bY_2^2 - aY_2^{-1} \\ &e_2(1): && aY_2^{-2} + bY_2^1 \\ &e_2(2): && bY_2^{-2} - aY_2^1. \end{aligned} \tag{3}$$

In terms of the multipole functions used in the refinements, the densities corresponding to these functions are

$$a_1: \qquad Y(00) + \frac{\sqrt{20}}{7}Y(20) + \sqrt{\frac{20}{63}}Y(40) \tag{4}$$

$$\mathrm{e}(1): \quad Y(00) - \frac{\sqrt{5}}{7}(2aa^* - bb^*)Y(20) + \frac{1}{7}(aa^* - 4bb^*)Y(40) + \sqrt{\frac{5}{14}}\left[(ab^* + a^*b)Y(43+) + \mathrm{i}((ab^* - a^*b)Y(43-)\right] \tag{5}$$

$$\mathrm{e}(2): \quad Y(00) + \frac{\sqrt{5}}{7}(aa^* - 2bb^*)Y(20) - \frac{1}{7}(4aa^* - bb^*)Y(40) - \sqrt{\frac{5}{14}}\left[(ab^* + a^*b)Y(43+) + \mathrm{i}((ab^* - a^*b)Y(43-)\right]. \tag{6}$$

The densities of degenerate functions with e_1 and e_2 representations are identical. The multipole parameters obtained in the unrestricted refinement are compatible with 25% of the magnetization being due to electrons in the a_1 orbitals and 75% to those in the e(1) orbitals. The phases of the e functions can be chosen such that a is real, in which case $a = 0.95$, $b = 0.22(1 + \mathrm{i})$. These results indicate that the electrons giving rise to the susceptibility are mostly in V 3d orbitals with $l_z = \pm 2$.

It should perhaps be pointed out that all of the V multipole functions used to model the data are centrosymmetric and cannot therefore reproduce the strongly acentric features of the ME reconstruction (figure 1). The acentricity is much more marked in the high-temperature susceptibility than in that measured at 180 K. The principal change observed in the structure of V_2O_3 between 180 and 600 K is an increase in the metal–metal distances by about 0.04 Å although the metal–oxygen distances increase by less than half this amount [7]. These changes, linked with the increased resistivity, have been taken to indicate an increase in the local metal–oxygen interactions and a decrease in the metal–metal interactions with a corresponding diminution in the density of states at the Fermi surface. The increased acentricity of the magnetization could also be due to increased metal–oxygen interaction since the oxygen octahedra which coordinate the metal ions are acentric.

According to Mattheiss [10] the band structure shows no obvious signs of an impending instability, and he therefore suggests that the changes in structure and transport properties may be due to development of cation vacancies and interstitial defects at high temperature. Our results can be interpreted reasonably in the light of this suggestion. Although the neutron data give no direct evidence for cation vacancies or interstitials, the presence of metal atoms at the interstitial positions on the triad axis would lead to increased acentricity in the magnetization distribution. Mattheiss' calculations show that the vacancy–interstitial perturbation of the band structure is especially strong and leads to a reduction in the DOS at the Fermi level. This perturbation also gives rise to significant modification in the relative energies of the different sub-bands; a result which can be correlated with the increased mixing between the e_g and t_{2g} sub-bands evident in the magnetization distribution.

Whatever the cause, the present results show that the electronic states which can be magnetized by an applied field at 600 K differ in form from those which are active at 180 K. They can no longer be described by functions corresponding to a trigonal perturbation of an octahedral field. At high temperatures there is sufficient mixing between e_g and t_{2g} states transforming according to the same trigonal representations that the resulting magnetization has nearly cylindrical symmetry about the triad axis and is due primarily to V 3d electrons in states with $l_z \pm 2$.

5. Conclusions

It has been shown that the magnetization which can be induced by an applied field in the high-temperature insulating phase of V_2O_3 at 600 K differs in form from that obtained in the

metallic phase at 180 K. At both temperatures a reverse polarization is induced around the O^{2-} ions; at 600 K it is 5% of the V moment compared to 6% at 180 K. On the other hand the high-temperature magnetization has nearly cylindrical symmetry about the triad axis and, in contrast with that obtained at 180 K, is very significantly acentric with respect to the cation site. This result suggests that the axial components of the molecular field effective at 600 K are considerably stronger than those at 180 K. These changes in magnetization distribution are consistent with the appearance of cation disorder with increasing temperature in V_2O_3 which has been invoked by Mattheiss [10] to account for the changes in the transport and thermodynamic properties.

Acknowledgments

We are grateful to Eddy Lelièvre Berna, Eric Bourgeat Lami and Serge Pujol for their work in developing the high-temperature insert, for the 10 T superconducting magnet, without which this experiment would not have been possible.

References

[1] Paolasini L, Vettier C, de Bergevin F, Yakhou F, Mannix D, Neubeck W, Stunault A, Altarelli M, Fabrizio M, Metcalf P A and Honig J M 2000 *Physica* B **281+282** 485
[2] Bao W, Broholm C, Aeppli G, Dai P, Honig J M and Metcalf P 1997 *Phys. Rev. Lett.* **78** 507
[3] Brown P J, Costa M M R and Ziebeck K R A 1998 *J. Phys.: Condens. Matter* **10** 9581
[4] Kuwamoto H, Honig J M and Aeppli 1980 *Phys. Rev.* B **22** 2626
[5] Jayaraman A, McWhan D B, Remeika J P and Dernier P D 1970 *Phys. Rev.* B **2** 3751
[6] Menth A and Remeika J P 1970 *Phys. Rev.* B **2** 3756
[7] Robinson W R 1975 *Acta Crystallogr.* B **31** 1160
[8] Gull S F and Daniel G J 1989 *Quantified Maximum Entropy 'MEMSYS 3' Users Manual* Maximum Entropy Data Consultants Limited, 33 North End, Meldreth Royston SG8 6NR, UK
[9] Marshal W and Lovesey S W 1971 *Theory of Thermal Neutron Scattering* (Oxford: Oxford University Press) p 132
[10] Mattheiss L F 1994 *J. Phys.: Condens. Matter* **6** 6477